Applied Physics Express 12, 062007 (2019)
https://doi.org/10.7567/1882-0786/ab1e92

LETTER

Infrared thermometry for breakage detection of optical fibers embedded in structures

Yosuke Mizuno[1*], Sonoko Hagiwara[1], Heeyoung Lee[1], Yutaka Ochi[2], Takahiro Matsui[3], Yukihiro Matsumoto[4], Yosuke Tanaka[5], Hitoshi Nakamura[6], and Kentaro Nakamura[1]

[1]Institute of Innovative Research, Tokyo Institute of Technology, Yokohama 226-8503, Japan
[2]Advanced Composites Center, Toray Industries, Inc., Nagoya 455-0024, Japan
[3]First Advanced Composites Technical Department, Toray Industries, Inc., Nagoya 455-0024, Japan
[4]Department of Architecture and Civil Engineering, Toyohashi University of Technology, Toyohashi, Aichi 441-8580, Japan
[5]Institute of Engineering, Tokyo University of Agriculture and Technology, Koganei, Tokyo 184-8588, Japan
[6]Department of Civil and Environmental Engineering, Tokyo Metropolitan University, Hachioji, Tokyo 192-0397, Japan

*E-mail: ymizuno@sonic.pi.titech.ac.jp

Received March 26, 2019; revised April 16, 2019; accepted May 1, 2019; published online May 20, 2019

We show that infrared thermometry can be used to detect a breakage point in an optical fiber embedded in a structure. Around the breakage point, incident light induces heat, which is detected using an infrared thermometer. By this method, we can obtain position information of a breakage point, including accurate information on where it is located in the actual structure, on a real-time basis. We experimentally show the practical usefulness of this method by detecting a breakage point in an optical fiber embedded in a composite structure comprising carbon fiber-reinforced plastics.

Health monitoring of civil infrastructure such as buildings, tunnels, bridges, dams, levees, pipelines, wind turbines, and railroad tracks, has become one of the most important research topics in modern society. To date, as structural monitoring tools, optical fiber sensors have been extensively studied and applied to the measurement of strain,[1–4] temperature,[1–4] pressure,[5,6] stress,[7,8] humidity,[9,10] acoustic impedance,[11,12] and many others. Needless to say, these physical parameters can be correctly measured under the assumption that the optical fibers embedded in structures have no breakage points. Once part of the embedded fiber is cut by large shear stress, etc., it becomes difficult to continue most of these measurements. Especially when the sensor is a two-end-access type, in which two light beams need to be injected into both ends of the fiber under test, one breakage point completely disables its operation. Even if the sensor is a single-end-access type, no information can be obtained from the distal part of the breakage. Thus, breakage of an embedded fiber should be avoided, but in case it is accidentally caused for some unavoidable reason, the breakage point should be detected as soon as possible.

We can obtain position information on the breakage point of an embedded optical fiber using single-end-access distributed loss sensors, such as optical time-domain reflectometry,[13–17] optical frequency-domain reflectometry,[18–22] and optical correlation-domain reflectometry.[23–28] Optical interferometry based on multiple Fresnel reflections[29] and some of the distributed strain sensors[30] can also be used for this purpose. All of these sensors can determine the position of the breakage point with high sampling rates and high spatial resolutions; the system cost has also been decreasing. However, at the site of the actual measurement, these methods suffer from a serious issue from a practical viewpoint: even if we obtain the information that the embedded fiber has a breakage point, for example, 13.5 m away from a certain point, it is difficult to know immediately which part of the actual structure that point is located in.

In this paper, to resolve this practical problem, we develop a new method, using an infrared thermometer (IRT) to detect a breakage point in an optical fiber embedded in a structure. The principle is simple—at the breakage point of an optical fiber, optical energy is converted into thermal energy, heating the surrounding part of the structure, which is detected using an IRT. By this method, we can obtain the position information of a breakage point, including accurate information on where it is in the actual structure, on a real-time basis with high cost efficiency. We show the practical usability of this method by detecting a breakage point in an optical fiber embedded in a composite structure comprising a steel plate and carbon fiber-reinforced plastic (CFRP) strips.

At a breakage point in an optical fiber, the optical energy is converted into thermal energy and heats the surrounding structural area. Here, we give a simple quantitative expression employing a model based on Newton's law of cooling.[31] Suppose light is incident at $t = 0$, the temperature at the breakage point $T(t)$ is given by

$$T(t) = T(0) + \frac{Q}{hA}\left\{1 - \exp\left(-\frac{hA}{C}t\right)\right\}, \tag{1}$$

where Q is the thermal energy, h is the heat transfer coefficient, A is the heat transfer surface area, and C is the heat capacity of the structure; $T(0)$ corresponds to room temperature. It is notable that, at $t \to \infty$, the increase in temperature is proportional to Q, i.e. the power of the incident light.

The temperature at the breakage point can be roughly measured with an IRT. In general, a blackbody is a perfect absorber of any radiation incident on it and can emit radiation.[32,33] When heated, it generates blackbody radiation, the characteristics of which depend only on temperature. The total radiant emittance W of an object (both blackbody and non-blackbody) is given by the Stefan–Boltzmann law as

$$W = \varepsilon\sigma T^4, \tag{2}$$

where ε is the emissivity of the object (1 for a blackbody), σ is the proportional constant, and T is the surface temperature of the object. By measuring the infrared energy emitted by the object, its temperature can be determined. The surface temperature of a heated part of a structure can thus be

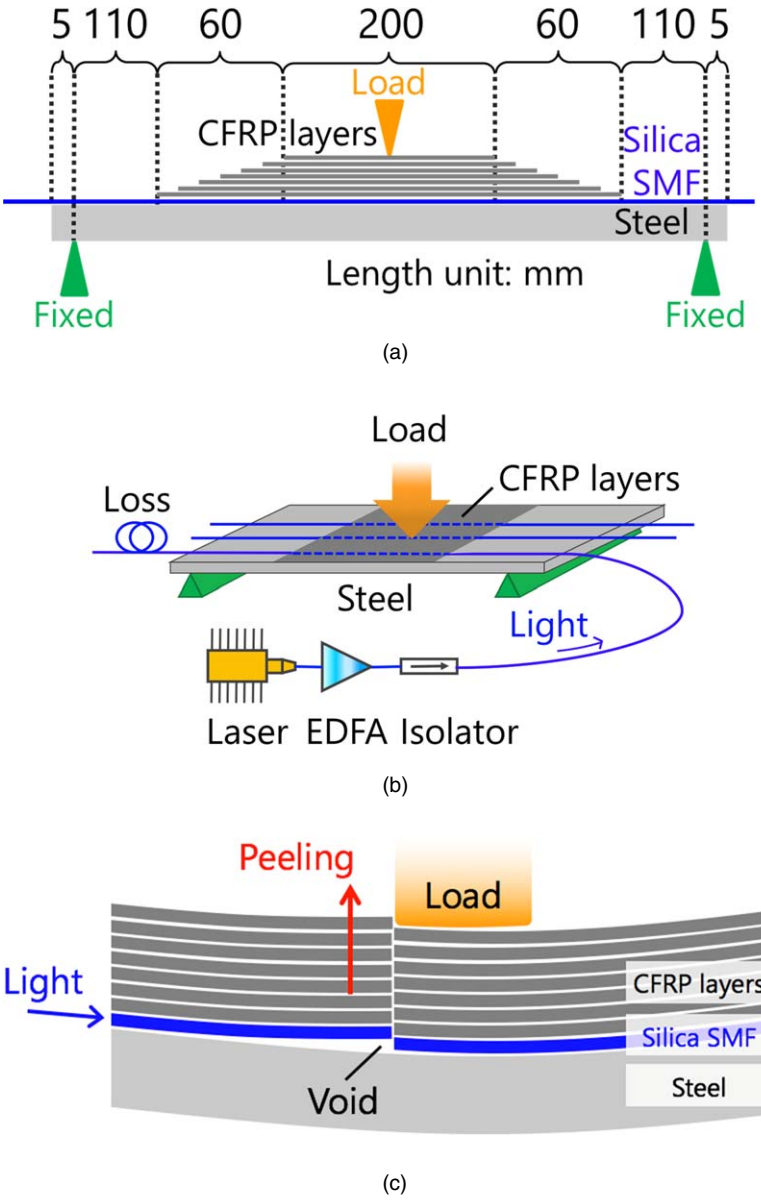

Fig. 1. (Color online) (a) Sample geometry. (b) Experimental setup. EDFA: erbium-doped fiber amplifier. (c) Schematic of fiber breakage caused by peeling of CFRP strips.

measured with an IRT. Though this method suffers from a relatively large temperature error caused by the surface state of the object (resulting in different ε values), it has advantages such as cost efficiency, real-time operation, and visual display of the heat.

Owing to their high strength, high elastic modulus, light weight, and high corrosion resistance, CFRPs have been used as materials for repairing or strengthening steel structures.[34] In this experiment, as a specimen, a CFRP-strengthened steel plate was fabricated using what is called a vacuum-assisted resin transfer molding (VaRTM) technique,[35–38] which is known as a reliable method for fabricating composite materials. The VaRTM process was performed by infusing a liquid resin into laminated fibers or woven fabrics exploiting the pressure difference between atmosphere and vacuum; the resin was then hardened by heat (see Refs. 35 and 36 for more details).

Figures 1(a) and 1(b) show the schematic structures of the specimen. Three pieces of 1.4-m-long silica single-mode fibers (SMFs; core diameter: 8 μm, cladding diameter: 125 μm, outer diameter: 250 μm) were embedded in parallel between a steel plate and CFRP strips [containing carbon fiber cloth (UM46-40G, Torayca)]. The intervals between the three SMFs were 9 mm, and the lengths of the embedded fiber sections were all 320 mm. This structure was fabricated by placing the SMF before the infusing liquid resin during the VaRTM process. The depth of the structure (both the steel plate and the CFRP strips) was 39 mm, and the thickness of the steel plate was 12 mm. The total thickness of the CFRP strips involving seven tapered layers (the length of each strip differed by 10 mm) was approximately 3 mm.

To break the embedded fibers by peeling of the CFRP strips, large compressive strain was applied to the middle of the specimen by tightening a top screw of a three-point bending device (Fig. 3). After breakage, we injected light into one of the SMFs embedded on the sides of the specimen (Fig. 2). The light source was a semiconductor laser at 1551 nm, and its output power was amplified to 15–27 dBm using an erbium-doped fiber amplifier. The surface temperature of the CFRP strips was then measured with an IRT

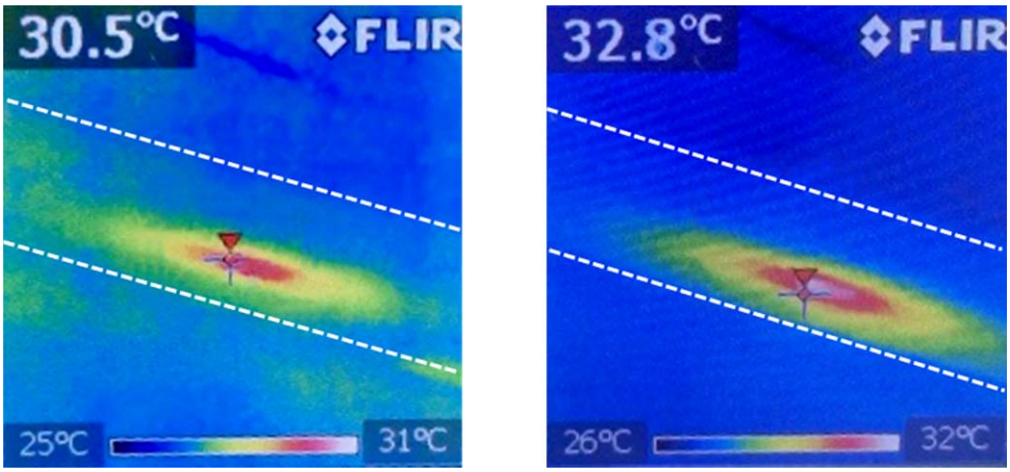

Fig. 2. (Color online) IRT images taken (a) 30 s and (b) 180 s after light injection at 27 dBm. The dotted lines are the boundaries of the surface of the specimen.

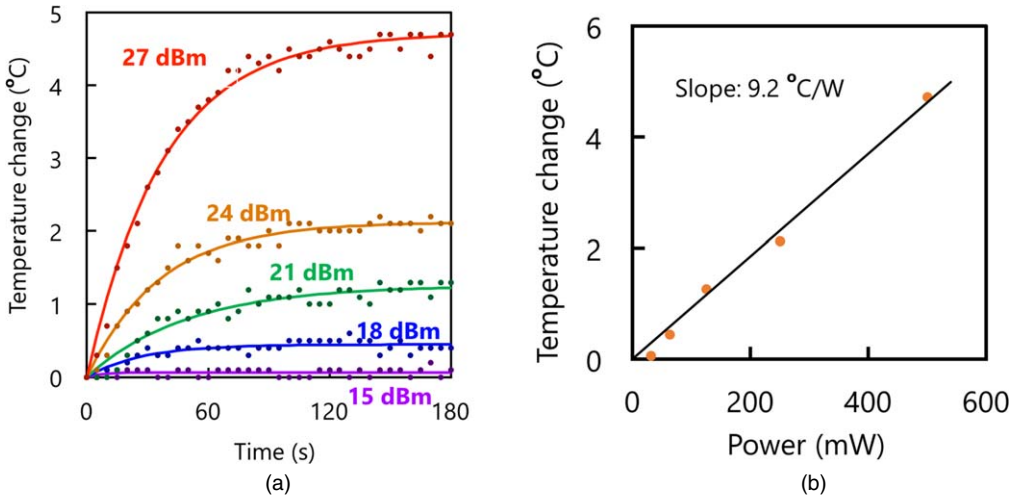

Fig. 3. (Color online) (a) Temporal variations of temperature change at five different incident powers. The solid curves are exponential fits. (b) Temperature change (180 s after light injection) plotted as a function of incident power. The solid line is a linear fit.

(FLIRi7, FLIR). The emissivity of the CFRP surface was set to 0.85, and the room temperature was 28 °C.

The IRT images taken 30 s and 180 s after light at 27 dBm (=500 mW) was injected are shown in Figs. 2(a) and 2(b), respectively. A clear heated spot was detected on the side of the specimen, and its central position agreed with the breakage point of the embedded SMF. The shape of the heated area was not completely circular but highly elliptic, because of the thermal anisotropy of the CFRP strips. As time proceeded, the temperature at the hottest part increased.

Subsequently, we measured the temporal dependencies of the temperature change at the heated spot when the incident optical power was varied [Fig. 3(a)]. Regardless of the incident power, by lapse of time, the temperature change increased and became almost constant at approximately 150 s after light injection. These trends were well fitted by exponential curves, as suggested by Eq. (1). The temperature change at the same timing was larger as the incident power was higher.

Finally, we plotted the saturated temperature change, defined as the temperature change 180 s after light injection, as a function of the incident optical power [Fig. 3(b)]. Note that the optical power on the horizontal axis is indicated using a linear unit (mW). With increasing incident power, the temperature linearly increased with a coefficient of 9.2 °C W^{-1}. This linear trend agrees with the aforementioned theory. Thus, higher-power light injection was shown to enable detection of a breakage point with a higher contrast.

In conclusion, we demonstrated IRT-based detection of a breakage point of an optical fiber embedded in a structure. Using an IRT, we simply detect the heated area of the structure around the breakage point of the fiber. The unique advantage of this method is that we can obtain the position information of a breakage point, including accurate information on where it is located in the actual structure. Other advantages are its real-time operation and cost efficiency. We showed the practical usefulness of this method by detecting a breakage point of a fiber embedded in a CFRP-based structure. The obtained quantities, such as the time constant (~150 s) and the dependence coefficient (9.2 °C W^{-1}), will vary according to the materials and conditions of the structure in which optical fibers are embedded. In particular, when optical fibers are embedded deep in structures, this method will be less effective. Injection of extremely high-power light

may enhance the limited depth to some extent, but it is not cost-effective and sometimes causes a so-called fiber fuse phenomenon.[39,40] These points need to be quantitatively analyzed further in the future. We believe that, nevertheless, our IRT-based technique remains of significant use in detecting fiber breakages on site. Note that this technique may also be useful for detecting extremely high optical loss caused locally when a crack is induced in the fiber-embedded structure.

Acknowledgments This work was supported by the MLIT Construction Technology Research and Development Subsidy Program, by JSPS KAKENHI Grant Numbers 17H04930 and 17J07226, and by a research grant from the Fujikura Foundation.

ORCID iDs Yosuke Mizuno https://orcid.org/0000-0002-3362-4720 Heeyoung Lee https://orcid.org/0000-0003-3179-0386 Yosuke Tanaka https://orcid.org/0000-0002-6539-5977 Kentaro Nakamura https://orcid.org/0000-0003-2899-4484

1) A. H. Hartog, *An Introduction to Distributed Optical Fibre Sensors* (CRC Press, Boca Raton, FL, 2017).
2) R. Kashyap, *Fiber Bragg Gratings* (Elsevier, New York, 1999).
3) Y. Mizuno, N. Hayashi, H. Fukuda, K. Y. Song, and K. Nakamura, Light: Sci. Appl. **5**, e16184 (2016).
4) D. Zhou, Y. Dong, B. Wang, C. Pang, D. Ba, H. Zhang, Z. Lu, H. Li, and X. Bao, Light: Sci. Appl. **7**, 32 (2018).
5) R. Ishikawa, H. Lee, A. Lacraz, A. Theodosiou, K. Kalli, Y. Mizuno, and K. Nakamura, IEEE Photonics Technol. Lett. **29**, 2167 (2017).
6) Y. Mizuno, H. Lee, N. Hayashi, and K. Nakamura, Appl. Phys. Express **11**, 012502 (2018).
7) T. H. Chua and C. L. Chen, Appl. Opt. **28**, 3158 (1989).
8) T. Saida and K. Hotate, IEEE Photonics Technol. Lett. **9**, 484 (1997).
9) P. Kronenberg, P. K. Rastogi, P. Giaccari, and H. G. Limberger, Opt. Lett. **27**, 1385 (2002).
10) C. Bian et al., Appl. Opt. **57**, 356 (2018).
11) G. Bashan, H. H. Diamandi, Y. London, E. Preter, and A. Zadok, Nat. Commun. **9**, 2991 (2018).
12) D. M. Chow, Z. Yang, M. A. Soto, and L. Thévenaz, Nat. Commun. **9**, 2990 (2018).
13) M. K. Barnoski and S. M. Jensen, Appl. Opt. **15**, 2112 (1976).
14) G. P. Lees, H. H. Kee, and T. P. Newson, Electron. Lett. **33**, 1080 (1997).
15) M. Zoboli and P. Bassi, Appl. Opt. **22**, 3680 (1983).
16) P. Healey and P. Hensel, Electron. Lett. **16**, 631 (1980).
17) Q. Zhao et al., Sci. Rep. **5**, 10441 (2015).
18) W. Eickhoff and R. Ulrich, Appl. Phys. Lett. **39**, 693 (1981).
19) D. Uttam and B. Culshaw, J. Lightwave Technol. **3**, 971 (1985).
20) B. Soller, D. Gifford, M. Wolfe, and M. Froggatt, Opt. Express **13**, 666 (2005).
21) S. Venkatesh and W. V. Sorin, J. Lightwave Technol. **11**, 1694 (1993).
22) F. Ito, X. Fan, and Y. Koshikiya, J. Lightwave Technol. **30**, 1015 (2012).
23) R. C. Youngquist, S. Carr, and D. E. N. Davies, Opt. Lett. **12**, 158 (1987).
24) E. A. Swanson et al., Opt. Lett. **17**, 151 (1992).
25) Z. He and K. Hotate, J. Lightwave Technol. **20**, 1715 (2002).
26) K. Hotate, M. Enyama, S. Yamashita, and Y. Nasu, Meas. Sci. Technol. **15**, 148 (2004).
27) M. Shizuka, S. Shimada, N. Hayashi, Y. Mizuno, and K. Nakamura, Appl. Phys. Express **9**, 032702 (2016).
28) M. Shizuka, N. Hayashi, Y. Mizuno, and K. Nakamura, Appl. Opt. **55**, 3925 (2016).
29) Y. Mizuno, N. Hayashi, and K. Nakamura, J. Lightwave Technol. **32**, 4734 (2014).
30) Y. Mizuno, N. Hayashi, H. Fukuda, and K. Nakamura, Jpn. J. Appl. Phys. **56**, 072501 (2017).
31) I. Newton, Philos. Trans. R. Soc. London **22**, 824 (1701) [in Latin].
32) H. Krips, Stud. Hist. Philos. Sci. A **17**, 43 (1986).
33) N. Hayashi, Y. Mizuno, and K. Nakamura, Appl. Phys. Express **6**, 076601 (2013).
34) N. Uddin, *Developments in Fiber-Reinforced Polymer (FRP) Composites for Civil Engineering* (Woodhead Publishing, Oxford, 2013).
35) L. Y. Lin, J. H. Lee, C. E. Hong, G. H. Yoo, and S. G. Advani, Comp. Sci. Technol. **66**, 2116 (2006).
36) N. Takeda, Int. J. Fatigue **24**, 281 (2002).
37) S. Shimada et al., Electron. Lett. **52**, 1472 (2016).
38) H. Lee et al., Appl. Phys. Express **11**, 072501 (2018).
39) R. Kashyap, Opt. Express **21**, 6422 (2013).
40) Y. Mizuno, N. Hayashi, H. Tanaka, K. Nakamura, and S. Todoroki, Appl. Phys. Lett. **104**, 043302 (2014).